INTL JOURNAL OF ELECTRONICS AND TELECOMMUNICATIONS, 2026, VOL. 72, NO. 2, PP. 1-8
Manuscript received February 13, 2026; revised April 2026. doi: 10.24425/ijet.2026.157904

Development and evaluation of Gradient-Based Numerical Algorithms for object localization in multistatic passive radar system

Piotr Szelągowski

***Abstract*—Passive radar does not transmit its own signals but relies on external sources of illumination. Estimating a target position requires distance measurements from at least three spatially separated sensors. This paper presents an adaptation of a maximum likelihood estimator (MLE) for target localization using multiple (three or more) bistatic range or DToA (Difference Time of Arrival) measurements. The Gauss–Newton, Levenberg, and Levenberg–Marquardt methods are compared with respect to numerical stability and localization accuracy under different noise levels and initialization conditions.**

***Keywords*—passive radar; multistatic radar system; Gauss-Newton algorithm; Levenberg-Marquardt algorithm; Maximum Likelihood Estimator; MLE**

I. Introduction

PASSIVE radar systems have attracted increasing attention in recent years due to their ability to detect and track objects without transmitting dedicated signals, thereby providing significant advantages in terms of low probability of intercept, enhanced survivability, and reduced operational costs. In military applications, one of the principal advantages of passive radar is the absence of active emissions, which substantially complicates detection and countermeasure (ECM) deployment. These systems exploit existing radio-frequency transmissions, such as commercial broadcast and communication signals, as illuminators of opportunity [1]. By processing the reflections of these signals from targets, passive radars are capable of estimating target position, velocity, and other relevant parameters. Several fundamental challenges arise in passive radar systems, including [2,3]:

- signal quality and availability,
- multipath propagation and clutter suppression,
- calibration and time synchronization,
- direct-path interference in the surveillance channel,
- false alarm mitigation,
- multi-sensor data fusion.

A common approach to address these challenges is the use of multistatic passive radar architectures with multiple illuminators and/or receivers. In practical scenarios, multiple target detections are obtained from multiple sensors (transmitter–receiver or receiver–receiver pairs). In MIMO radar systems, information from ECM sensors [4-6], including Identification Friend or Foe (IFF) and Electronic Intelligence (ELINT), can also be used to enhance target localization [7].

This paper focuses on the final stage of passive radar signal processing: data fusion, which aims to produce a consistent and stable air situation picture from heterogeneous measurement sources. In multistatic passive radar systems, data fusion encompasses several key areas, including measurement association [8-9], target position estimation [7,10-12], and tracking [13-15], which have already been described in the literature. Specifically, we address the problem of estimating the coordinates of airborne targets based on measurements collected by multiple sensors and associated with individual objects.

II. Problem formulation

Multistatic radar refers to a system architecture in which multiple receivers (passive radar nodes) and multiple transmitters (e.g., illuminators of opportunity or onboard aircraft emitters) are spatially distributed. This setup creates a complex sensing environment, offering improved spatial coverage and enhanced target localization. However, it also brings significant challenges, particularly in achieving unambiguous localization of detected objects [8-9].

Fig. 1 illustrates an example geometry of a multistatic system, utilizing reflections from illuminators of opportunity as well as signals emitted by the target itself.

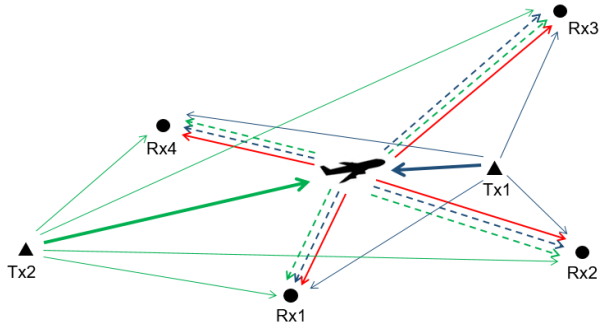

Fig. 1. Multistatic system geometry

Author is with PIT-RADWAR S.A., Poland (e-mail: piotr.szelagowski@pitradwar.com).

The primary challenge stems from the fact that each bistatic transmitter–receiver pair defines a locus of possible target positions rather than a single point. Accurate localization therefore necessitates the combination of measurements from multiple transmitters and receivers, typically through multilateration [12], to intersect these loci and estimate the target coordinates. Consequently, the multistatic configuration gives rise to a nonlinear estimation problem, where integrating heterogeneous measurements requires advanced optimization and data fusion techniques to resolve ambiguities and ensure reliable target localization.

Bistatic range measurements are described below as typical for reflections from illuminators of opportunity, whereas DToA (Differential Time of Arrival) measurements represent a typical observation of signals emitted directly by the target.

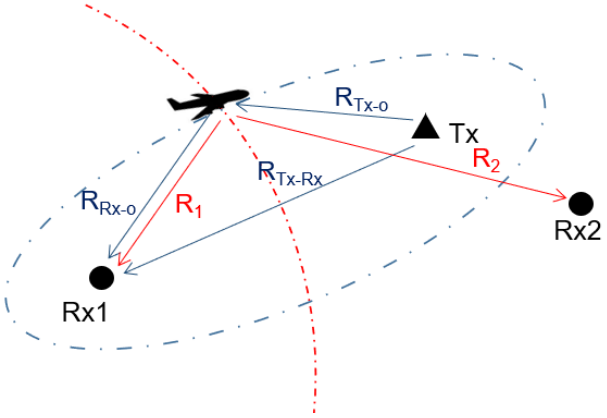

Fig. 2. Bistatic range measurement and DToA range measurement geometry

The bistatic range is defined as the sum of the propagation distances from the transmitter to the target and from the target to the receiver, minus the direct distance between the transmitter and the receiver [16]. Each measurement corresponds to an ellipsoidal surface in Cartesian space, where the transmitter and receiver serve as the foci of the ellipsoid (Fig.2). As the positions of both the transmitter and receiver are known, the direct baseline distance between them is excluded in the subsequent analysis (1)(2):

$$R_{B_i}=R_{Tx_i\text{-}o}+R_{Rx_j\text{-}o}-R_{Tx_i\text{-}Rx_j} \quad (1)$$

$$R_{B_i}=R_{Tx_i\text{-}o}+R_{Rx_j\text{-}o} \quad (2)$$

where:

- $R_{Tx_i\text{-}o}$– Euclidean distance between the transmitter and the target
- $R_{Rx_j\text{-}o}$– Euclidean distance between the receiver and the target
- $R_{Tx_i\text{-}Rx_j}$– Euclidean distance between the transmitter and the receiver.

The DToA range is defined as the difference between the signal propagation paths from the target to two spatially separated receivers, namely the path to a given receiver minus the path to a designated reference receiver (3):

$$R_{DToA}=R_1-R_2 \quad (3)$$

where:

- R_1– Euclidean distance between the receiver and the target
- R_2– Euclidean distance between the reference receiver and the target.

This quantity represents the relative propagation delay of signals emitted by the same source and received at two distinct sensing elements, as commonly employed in onboard or electronic reconnaissance systems. Each DToA measurement defines a branch of a two-sheet hyperboloid in Cartesian space, with the receiver and the reference receiver acting as the foci (Fig.2).

Assume that n range-related measurements of a target are available, obtained from $n$spatially distinct transmitter–receiver or receiver–reference receiver pairs. In theory, target localization using bistatic and DToA measurements can be formulated as finding a point that simultaneously satisfies $n$geometric constraints, each corresponding to a surface defined by an individual sensor pair. This leads to a nonlinear system of equations, as shown in (4),

$$\begin{cases} R_1=F_1(x,y,z) \\ \dots \\ R_n=F_n(x,y,z) \end{cases} \quad (4)$$

where each observation $R_{i=1\dots n}$ represents either a bistatic range (path sum)(2) or a DToA measurement (path difference)(3).

In practical scenarios, measurements are subject to varying uncertainties, and the associated observation models F_i may differ. As a result, the exact intersection of all surfaces rarely yields an optimal estimate in a statistical sense. The localization task therefore involves heterogeneous measurement models and non-uniform noise characteristics, described by individual standard deviations σ_i. When more than three measurements are available, system (4) becomes overdetermined. Moreover, due to measurement noise, it is generally inconsistent, meaning that no exact solution exists. Consequently, target position estimation is formulated as an optimization problem, where the goal is to determine the position that minimizes an appropriate error criterion, most commonly the mean squared residual.

III. Analythical and Numerical Methods for Solving the Problem

In multistatic radar systems, targets may be observed by different numbers of data sources—such as transmitter–receiver or receiver–reference receiver pairs—at various times, resulting in varying levels of measurement redundancy.

The choice between analytical and numerical localization methods depends on the characteristics of the available data and the operational requirements of the system. Analytical methods attempt to solve the system of equations derived from the measurements directly, providing exact solutions when the system is well-determined, i.e., when exactly three independent measurements are available. These methods rely on algebraic manipulations to explicitly compute the target coordinates from the measurements. However, their performance deteriorates in the presence of noise, measurement errors, or redundant observations.

Numerical methods, although computationally more demanding, offer greater robustness and flexibility in practical applications. They are particularly well-suited for overdetermined systems, heterogeneous measurement accuracies, and noisy data. Techniques such as least squares, weighted least squares, and Maximum Likelihood Estimation (MLE) allow for effective fusion of measurements from multiple sources, mitigating the impact of measurement errors and providing more accurate and reliable target position estimates [17]. The application of the Gauss–Newton algorithm for object position estimation in multistatic passive radar systems is discussed in [18,19]. These factors motivate the focus on numerical methods, which will be examined in detail in the following section.

Due to the high combinatorial complexity associated with a large number of data sources, which is typical in multistatic radar systems, object localization can also be approached by discretizing the space into a grid and searching for intersections of measurements. This approach, analyzed in [20], presents significant challenges for real-time implementation and is therefore mainly suitable as a preliminary step prior to the final position estimation.

IV. MLE-Based Localization for Multistatic Passive Radar

This section introduces the target position estimator. Maximum Likelihood Estimation (MLE) is a widely used statistical method in fields such as navigation and econometrics and can be applied to radar systems to estimate target positions by maximizing the likelihood function over all available measurements. Previous studies have applied MLE to DToA-based localization [17, 21-22]. Here, we extend MLE to multistatic passive radar systems, incorporating both bistatic range and DToA range measurements. To the best of our knowledge, this approach has not been reported before. It enables the estimation of target positions for any combination of measurements (2), (3) and available transmitters and receivers, allowing the solution of system (4) even when analytical methods are not feasible. Assuming Gaussian-distributed measurement errors with known standard deviations, the Gauss–Markov theorem [22] ensures that the least squares estimator is the best linear unbiased estimator for linear models. Measurements with different variances should be appropriately weighted. Under the Gaussian assumption, the least squares and maximum likelihood approaches are equivalent. The estimator seeks the parameter vector β that minimizes the sum of squared residuals (5,6),

$$\hat{\beta} = \arg\min \mathrm{e}^T \mathrm{e} \tag{5}$$

$$\mathrm{e} = \mathrm{X} - F\hat{\beta} \tag{6}$$

where $\hat{\beta}$is the estimated parameter vector, e is the residual vector, $\mathrm{X} = [\hat{x}, \hat{y}, \hat{z}]^T$the estimated target position, and F *is* the measurement function. The corresponding linear estimator is (7).

$$\hat{\beta} = (F^T F)^{-1} F^T \mathrm{X}. \tag{7}$$

Because of the fact that F is nonlinear with respect to Cartesian coordinates, linearization is required. Partial derivatives of the bistatic and DToA range measurements are (8-15),

$$\frac{\partial F_{B_i}}{\partial \mathrm{x}} = \frac{\mathrm{x}-\mathrm{x}_{\mathrm{Tx}_i}}{\mathrm{R}_{\mathrm{Tx}_i\text{-}o}} + \frac{\mathrm{x}-\mathrm{x}_{\mathrm{Rx}_i}}{\mathrm{R}_{\mathrm{Rx}_i\text{-}o}} \tag{8}$$

$$\frac{\partial F_{B_i}}{\partial \mathrm{y}} = \frac{\mathrm{y}-\mathrm{y}_{\mathrm{Tx}_i}}{\mathrm{R}_{\mathrm{Tx}_i\text{-}o}} + \frac{\mathrm{y}-\mathrm{y}_{\mathrm{Rx}_i}}{\mathrm{R}_{\mathrm{Rx}_i\text{-}o}} \tag{9}$$

$$\frac{\partial F_{B_i}}{\partial \mathrm{z}} = \frac{\mathrm{z}-\mathrm{z}_{\mathrm{Tx}_i}}{\mathrm{R}_{\mathrm{Tx}_i\text{-}o}} + \frac{\mathrm{z}-\mathrm{z}_{\mathrm{Rx}_i}}{\mathrm{R}_{\mathrm{Rx}_i\text{-}o}} \tag{10}$$

$$\frac{\partial F_{DToA_i}}{\partial \mathrm{x}} = \frac{\mathrm{x}-\mathrm{x}_{\mathrm{Tx}_i}}{\mathrm{R}_{\mathrm{Tx}_i\text{-}o}} - \frac{\mathrm{x}-\mathrm{x}_{\mathrm{Rx}_i}}{\mathrm{R}_{\mathrm{Rx}_i\text{-}o}} \tag{11}$$

$$\frac{\partial F_{DToA_i}}{\partial \mathrm{y}} = \frac{\mathrm{y}-\mathrm{y}_{\mathrm{Tx}_i}}{\mathrm{R}_{\mathrm{Tx}_i\text{-}o}} - \frac{\mathrm{y}-\mathrm{y}_{\mathrm{Rx}_i}}{\mathrm{R}_{\mathrm{Rx}_i\text{-}o}} \tag{12}$$

$$\frac{\partial F_{DToA_i}}{\partial \mathrm{z}} = \frac{\mathrm{z}-\mathrm{z}_{\mathrm{Tx}_i}}{\mathrm{R}_{\mathrm{Tx}_i\text{-}o}} - \frac{\mathrm{z}-\mathrm{z}_{\mathrm{Rx}_i}}{\mathrm{R}_{\mathrm{Rx}_i\text{-}o}} \tag{13}$$

$$\mathrm{R}_{\mathrm{Tx}_i\text{-}o} = \sqrt{(\mathrm{x}-\mathrm{x}_{\mathrm{Tx}_i})^2 + (\mathrm{y}-\mathrm{y}_{\mathrm{Tx}_i})^2 + (\mathrm{z}-\mathrm{z}_{\mathrm{Tx}_i})^2} \tag{14}$$

$$\mathrm{R}_{\mathrm{Rx}_i\text{-}o} = \sqrt{(\mathrm{x}-\mathrm{x}_{\mathrm{Rx}_i})^2 + (\mathrm{y}-\mathrm{y}_{\mathrm{Rx}_i})^2 + (\mathrm{z}-\mathrm{z}_{\mathrm{Rx}_i})^2} \tag{15}$$

where:

- i is the measurement number, receiver number, i=1 … n
- j is the reference receiver number, j=1 … n.

A. Gauss-Newton method

The implementation of the MLE based on Gauss-Newton approach [18] is as follows (16–20):

$$\mathrm{X}^{(k+1)} = \mathrm{X}^{(k)} - \Delta\theta \tag{16}$$

$$\Delta\theta = -(J^{\mathrm{T}} W J)^{-1} J^{\mathrm{T}} W \mathrm{e} \tag{17}$$

$$W = \mathrm{diag}\left(\frac{1}{\sigma_1^2}, \ldots, \frac{1}{\sigma_n^2}\right) \tag{18}$$

$$\mathrm{e} = \begin{bmatrix} \mathrm{R}_{\mathrm{B}_1} - \hat{\mathrm{R}}_{\mathrm{B}_1} \\ \cdots \\ \mathrm{R}_{\mathrm{B}_n} - \hat{\mathrm{R}}_{\mathrm{B}_n} \end{bmatrix} \tag{18}$$

$$\hat{\mathrm{R}}_{\mathrm{B}_i} = \sqrt{(\hat{\mathrm{x}}-\mathrm{x}_{\mathrm{Rx}_i})^2 + (\hat{\mathrm{y}}-\mathrm{y}_{\mathrm{Rx}_i})^2 + (\hat{\mathrm{z}}-\mathrm{z}_{\mathrm{Rx}_i})^2} + \sqrt{(\hat{\mathrm{x}}-\mathrm{x}_{\mathrm{Tx}_i})^2 + (\hat{\mathrm{y}}-\mathrm{y}_{\mathrm{Tx}_i})^2 + (\hat{\mathrm{z}}-\mathrm{z}_{\mathrm{Tx}_i})^2} \tag{19}$$

where:

- $J^{(k)}$is the Jacobi matrix evaluated at $\mathrm{X}^{(k)}$,
- σ_i denotes the standard deviation of the i-th measurement,
- $W = Q^{-1}$is the weight matrix, with Qbeing the covariance matrix,
- $\Delta\theta$ is update step,
- k is the iteration index
- $\hat{\mathrm{R}}_{\mathrm{B}_i}$ is the estimated bistatic range or DToA range based on the value of $\mathrm{X}^{(k)}$.

The weight matrix (18) is constructed as the inverse covariance matrix of independent measurements, resulting in a diagonal matrix with entries equal to the reciprocal of the measurement variances. In certain cases, the Newton method may become unstable, especially when the initial guess is far from the true target position. To enhance stability, a step-size reduction coefficient α [19] is used, modifying the update as follows(20),

$$\Delta\theta = -\alpha(J^{\mathrm{T}} W J)^{-1} J^{\mathrm{T}} W \mathrm{e} \tag{20}$$

where $\alpha \in (0,1]$.

Reducing the step size limits large jumps between iterations, enhancing stability and reducing the risk of overshooting local minima, albeit at the cost of slower convergence. To prevent algorithm divergence more effectively than by employing a simple step-size reduction factor α, two alternative damping-based methods are presented below: the Levenberg algorithm and the Levenberg–Marquardt algorithm.

B. *Levenberg algorithm*

In practical nonlinear parameter estimation, the classical Newton method often encounters numerical instability, particularly when the Jacobian matrix is ill-conditioned or near singular. To address this issue, the Levenberg method [10] introduces a damping factor λ into the Gauss-Newton update equation (17), which regulates the step size and direction during iterations. The update rule is given by (21).

$$\Delta\theta = -(J^{\top}WJ + \lambda \mathrm{I})^{-1}J^{\top}W\mathrm{e} \qquad (21)$$

Large values of λ make the algorithm behave similarly to gradient descent algorithm [24], providing enhanced stability in regions far from the optimal solution. Small values of λ recover the behavior of the Gauss–Newton method, allowing faster convergence near the solution. The damping factor is usually selected heuristically and may require problem-specific tuning. The Levenberg method is particularly advantageous when stability is more critical than convergence speed, such as in problems with poor initial estimates or ill-conditioned Jacobi matrices.

C. *Levenberg-Marquardt algorithm*

The Levenberg–Marquardt (LM) algorithm [25] is an enhancement of the original Levenberg algorithm [23] incorporating adaptive damping and a diagonal approximation of the Hessian matrix. This modification improves both the robustness and the convergence rate of iterative parameter estimation. The LM update step is given by (22).

$$\Delta\theta = -\left(J^{\top}WJ + \lambda\,\mathrm{diag}(J^{\top}WJ)\right)^{-1}J^{\top}W\mathrm{e} \qquad (22)$$

Unlike the classical L method, LM dynamically adjusts the damping factor λ during iterations:

- if the cost function decreases, λ is reduced, allowing faster convergence (approaching the Gauss–Newton regime),
- if the cost function increases, λ is increased, improving stability (approaching the gradient descent regime).

This hybrid mechanism ensures reliable convergence even in regions with nearly flat likelihood surfaces or when the initial parameter estimates are far from the optimum. By combining the stability of Levenberg's method with the rapid convergence of Gauss–Newton, Levenberg-Marquardt has become a standard tool for nonlinear curve fitting, parameter estimation, and nonlinear localization problems, where both robustness and computational efficiency are critical.

V. RESULTS

The following section provides an overview of the research methodology and the results obtained, which form the basis for comparing and evaluating the considered algorithms, as well as for drawing the conclusions presented in the summary. This section presents the results of the proposed algorithms using simulated measurement data. For each test scenario, reference range measurements were calculated based on predefined positions of the receivers and transmitters (or reference receivers). Synthetic zero-mean noise was then added to simulate measurement uncertainty under varying accuracy levels. Subsection A presents results for bistatic range measurements, while Subsection B focuses on a case study involving the fusion of heterogeneous data sources, specifically bistatic range and DToA range measurements. Subsection C focuses on the accuracy of the obtained estimation results.

To evaluate the performance of the algorithms, a set of 20 object positions was randomly generated to collectively illustrate convergence behavior. The locations of the transmitters, receivers, and simulated objects are shown in Fig.3.

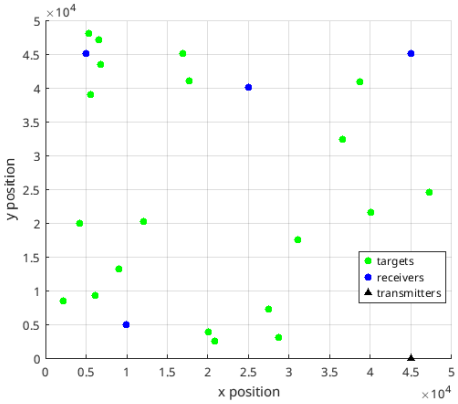

Fig. 3. Geometric configuration of the system showing transmitter, receiver, and target positions

The positions of the simulated objects are summarized in Table I, which provides, for each object, localization accuracy indices — GDOP, HDOP [26], and the HDOP/GDOP ratio. These indices indicate how measurement uncertainty propagates to the uncertainty of the estimated position. Due to the nearly coplanar geometry of the multistatic passive radar system and the lack of direct elevation (height) measurements, the HDOP/GDOP ratio was computed to assess whether the object's height can be reliably estimated in this scenario. A low HDOP/GDOP ratio (an engineering approximation can be introduced, indicating that this ratio is below 0.35) indicates poor observability of the target's vertical position component, which may lead to substantial dispersion in height estimates. The problem of poor observability of altitude is typical for multistatic passive radar [27] and results from the lack of direct measurement of the target's elevation angle, as well as the almost always coplanar arrangement of transmitters and receivers.

TABLE I.
OBJECT LOCATIONS AND COMPUTED POSITION ACCURACY METRICS

	x[m]	y[m]	z[m]	HDOP	GDOP	HDOP/GDOP ratio
1	5333	48095	1051	2,83	36,6	0,08
2	38746	40865	10556	2,29	2,48	0,92
3	4222	19989	3859	1,34	4,66	0,29
4	40003	21571	11017	2,57	4,57	0,56
5	9092	13190	2601	1,21	7,51	0,16
6	6803	43465	7377	2,42	4	0,61

7	27493	7248	10383	1,72	4,37	0,39
8	31103	17548	6646	1,28	2,89	0,44
9	20090	3798	3639	1,63	11,15	0,15
10	6166	9195	3639	1,62	10,06	0,16
11	20863	2483	10930	1,87	5,08	0,37
12	47239	24543	6382	3,89	7,7	0,51
13	16886	45003	5062	2,01	4,27	0,47
14	5560	39013	5287	2,09	3,4	0,61
15	12085	20196	2061	0,75	2,35	0,32
16	6599	47103	11517	2,83	4,12	0,69
17	28760	2989	3583	1,85	14,86	0,12
18	17658	41060	1169	1,57	10,8	0,15
19	2151	8450	8140	2,05	6,6	0,31
20	36586	32387	5960	1,43	2,05	0,70

A. Convergence analysis of the obtained results obtained for bistatic range measurements set case

To evaluate the localization performance of the methods described in Section 3, bistatic range measurement data were simulated independently for each of the 20 objects. For each object location, true bistatic range values were computed using four measurement sensors, corresponding to four transmitter – receiver pairs. Synthetic measurement datasets were then generated by adding zero-mean Gaussian noise with a known standard deviation of σ_{Rb} = 50 [m] to the true bistatic ranges. Object positions were repeatedly estimated based on four-measurement datasets. In each run, the initial point of the algorithm was randomly selected assuming a predefined maximum radius (r_{init}) value of the true object position. This procedure yielded results that provide a cross-sectional assessment of algorithm performance with respect to:

- various object locations (incuding various height observability, as show in Tab.1) ,
- varying measurement error levels across individual sensors,
- different algorithm initialization points.

To assess the performance of the algorithms, RMS error trajectories over successive iterations were compared and the overall percentage of consistent location estimates was evaluated. Consistency was defined using a criterion based on the Root Mean Square (RMS) value of the measurement residual vector (18). This criterion verifies whether a final estimate explains the measurement data at least as well as the reference (ground-truth) solution. In the other words, it evaluates the measurement consistency of the solution according to (23):

$$RMS(e) \leq RMS(e_{true}) \tag{23}$$

where:

$$e_{true} = \begin{bmatrix} R_{B_1}\text{-}R_{B_{1\_true}} \\ \cdots \\ R_{B_n}\text{-}R_{B_{n\_true}} \end{bmatrix}. \tag{24}$$

As previously reported in [6], in most cases satisfactory localization performance using the Gauss–Newton method is achieved within a few iterations, typically no more than five. Taking into account the introduced damping and the need for uniform visualization of the results, a fixed number of 10 iterations was adopted for all three algorithms. The initial value of the damping parameter was set to $\lambda = 0.1$. To show the results collectively, an envelope was used.

In the first stage, the initial estimate was assumed to be located close to the true target position. For successive runs of the algorithms, the starting points were randomly drawn within a radius of $r_{\text{init}} = 2$ [km] from the true object location. Fig. 4 and Fig. 5 illustrate the evolution of the localization error and the RMS of the measurement residuals (18) over successive iterations. The values at iteration equal to zero (x-axis) correspond to the initial estimates used to start the algorithms.

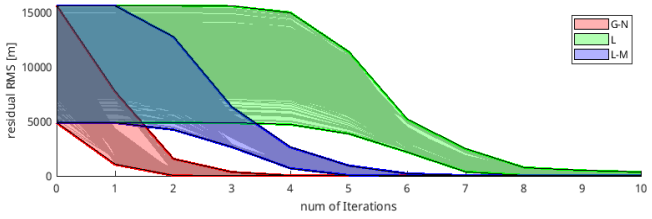

Fig. 4. Residual RMS value over successive iterations obtained from multiple simulation runs- default parameters (bistatic range measurement set case)

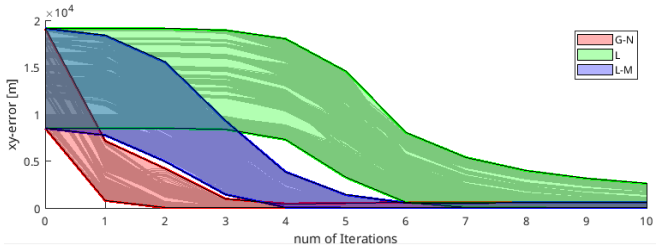

Fig. 5. Position error value over successive iterations obtained from multiple simulation runs- default parameters (bistatic range measurement set case)

It was observed that the damping factor in the Levenberg algorithm was excessively large; therefore, it was reduced by a factor of twenty, as specified in (25). With this setting, 100% of the estimates satisfied the adopted consistency criterion.

$$\Delta\theta = -(J^{\top}WJ + 0.05\lambda \mathrm{I})^{-1}J^{\top}W\mathrm{e} \tag{25}$$

Fig. 6 and Fig. 7 illustrate the evolution of the localization error and the RMS value of the measurement residuals (18) over successive iterations using lower damping formula in L method (25). Subsequently, the algorithms were evaluated in terms of the percentage of consistent estimates for progressively increasing initial position errors. The aggregated results are summarized in Table II.

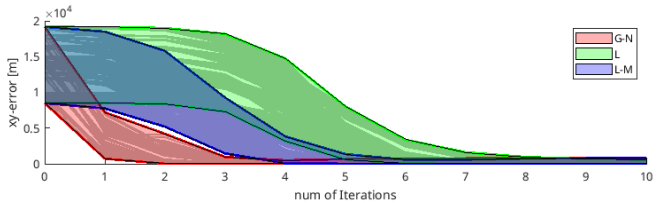

Fig. 6. Residual RMS value over successive iterations obtained from multiple simulation runs - reduced attenuation in the L algorithm (bistatic range measurement set case)

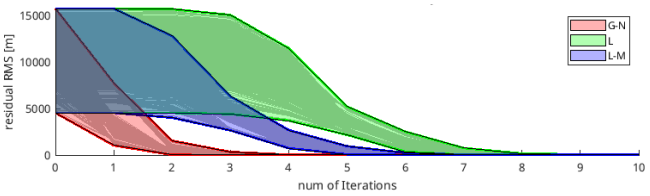

Fig. 7. Position error value over successive iterations obtained from multiple simulation runs- reduced attenuation in the L algorithm (bistatic range measurement set case)

TABLE II.
PERCENTAGE OF CONSISTENT ESTIMATES
(BISTATIC RANGE MEASUREMENT SET CASE)

	Estimate consistency rate [%]			
r_{init}[km]	GN (α = 1)	GN (α = 0.7)	L	LM
20	99	100	100	99
40	98	100	100	97
80	61	89	98	90
160	17	36	92	39

Furthermore, it was observed that, for the same value of the damping parameter λ, the Levenberg–Marquardt algorithm exhibits fluctuations more frequently than the Levenberg algorithm. An illustrative example of this behavior is shown in Fig. 8.

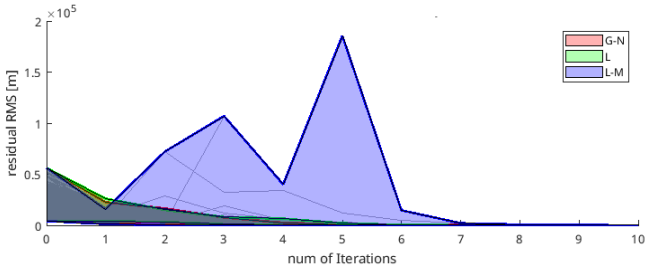

Fig. 8. Position error value over successive iterations obtained from multiple simulation runs- estimation fluctuations (bistatic range measurement set case)

B. Convergence analysis of the obtained results obtained for combinated bistatic range – DToA range measurements set case

In this subsection, an evaluation methodology analogous to that described in Subsection A was adopted, however, in this case, four bistatic range measurements and four DToA range measurements were simulated for four independent receiver pairs in each trial. The standard deviation of the DToA range measurements was set to σ_{DToA} = 50 [m]. In this variant, the number of measurements used for estimation is twice that of Scenario A. Consequently, improved localization accuracy can be expected, and the convergence behavior of the algorithms may differ from that observed in Scenario A.

In the first stage, the initial point of the algorithm was assumed to be located close to the true target position. In successive runs, the initial estimates were randomly selected within a radius of $r_{\text{init}} = 2$ [km] from the true position. Fig. 9 and Fig. 10 illustrate the evolution of the localization error and the RMS of the measurement residuals (18) over subsequent iterations.

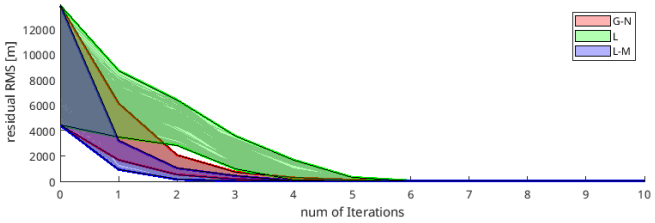

Fig. 9. Residual RMS value over successive iterations obtained from multiple simulation runs- default parameters (combinated bistatic range – DToA range measurements set case)

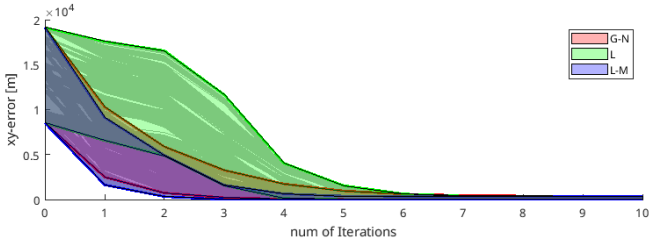

Fig. 10. Position error value over successive iterations obtained from multiple simulation runs- default parameters (combinated bistatic range – DToA range measurements set case)

The percentage of consistent estimates obtained in this scenario for increasing initial position errors is summarized in Table III. Overall, the results confirm the expected trend: target position estimation in Subsection B (bistatic range, DToA range measurements) exhibits better stability compared to Subsection A (only bistatic range measurements).

TABLE III.
PERCENTAGE OF CONSISTENT ESTIMATES (COMBINATED BISTATIC RANGE – DTOA RANGE MEASUREMENTS SET CASE)

	Estimate consistency rate [%]			
r_{init}[km]	GN (α=1)	GN (α=0.7)	L	LM
20	99	100	100	100
40	98	100	100	98
80	63	94	100	93
160	18	40	98	50

Another conclusion is that, based on the presented plots, the RMS of the measurement residual vector can serve as an indicator of estimation stability for real-time processing systems, since the patterns of the localization error plots and the RMS residual vector plots corresponds.

C. Accuracy analysis of the final estimates

In this section, localization error statistics were calculated for the scenarios described in Subsections A and B, as well as for their variants with increased measurement uncertainties. The obtained results are summarized in Table IV and Table V. The initial point of the algorithm was assumed to be located close to the true target position. For successive runs of the algorithms, the starting points were randomly drawn within a radius of $r_{\text{init}} = 2$ [km] from the reference location.

TABLE IV.
MEAN 3D LOCALIZATION ERROR

scenario parameters	mean 3D localization error (x,y,z) [m]		
	GN	L	LM
σ_{Rb} = 50 [m]	88.7	88.5	88.8
σ_{Rb} = 50 [m] σ_{DToA} = 50 [m]	65.6	65.5	65.6
σ_{Rb} = 100 [m]	188.2	179.2	189.8
σ_{Rb} = 100 [m] σ_{DToA} = 50 [m]	107.0	106.2	107.0

TABLE V.
MEAN HEIGHT ESTIMATION ERROR

scenario parameters	mean height estimation error (z) [m]		
	GN	L	LM
σ_{Rb} = 50 [m]	67.9	67.6	67.9
σ_{Rb} = 50 [m] σ_{DToA} = 50 [m]	49.8	49.7	49.8
σ_{Rb} = 100 [m]	143.8	134.7	145.5
σ_{Rb} = 100 [m] σ_{DToA} = 50 [m]	84.6	83.8	84.6

No significant differences were observed between the results obtained for the individual algorithms; however, in most cases, the smallest mean localization error was achieved using the Levenberg (L) method. Fig.11 presents box plots for one of the analyzed scenarios.

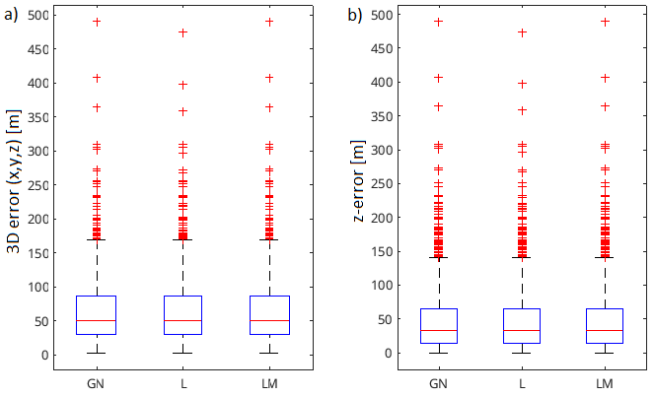

Fig 11. Box plots of: a) the 3D localization error and b) the vertical (z) localization error. Results obtained for scenario of $\sigma_{R_b} = 50$ [m] and $\sigma_{\mathrm{DToA}} = 50$ [m].

In Fig. 11, in addition to the previously reported mean values, the spread of the obtained results is also shown. A large number of outliers can be observed. These arise from the fact that a substantial part of the localization error is contributed by the z-axis component, and for several objects the height is poorly observable, as discussed earlier. This observation confirms that outliers appear to a similar extent in both the 3D localization error and the height error plots.

CONCLUSION

This paper addressed the problem of target position estimation in multistatic passive radar systems using bistatic range and DToA range measurements from multiple spatially distributed sources. Both analytical and numerical estimation methods were briefly discussed, and mathematical formulations of the Maximum Likelihood Estimator using the Gauss–Newton, Levenberg, and Levenberg–Marquardt algorithms were presented.

The performance of the algorithms was statistically evaluated using simulated data for targets at various positions within the radar coverage area, under different measurement error levels and algorithm initialization points. It was observed that the Gauss–Newton method requires additional damping to ensure convergence, without it, even small measurement errors may lead to non-convergent estimates. Among the tested approaches, the Levenberg algorithm (with reduced damping) achieved the highest percentage of consistent estimates for both the bistatic range measurement scenario and the combined measurement scenario. The accuracy of this method also proved to be the best among all three tested. Its computational complexity is comparable to the other methods, making it a suitable choice for practical applications in multistatic passive radar. No significant differences were observed between the algorithms in estimating target height along the Z-axis for the same starting points.

Overall, the study demonstrates that all three algorithms can be effectively applied to target localization in multistatic passive radar. Proper parameter selection ensures stable estimation across a wide range of target positions, but the risk of algorithm instability undoubtedly increases with the starting point error, thus numerical estimation can be recommended for use as the final processing step, with a pre-known starting point.

REFERENCES

[1] H. Griffiths and C. J. Baker, “An Introduction to Passive Radar, ser. Artech House radar series”. Boston: Artech House, 2017

[2] M. Weiss, “Guest Editorial: Multistatics and passive radar,” *IET Radar, Sonar & Navigation*, vol. 14, no. 12, pp. 1567–1570, 2024. https://doi.org/10.1049/rsn2.12683

[3] M. Asif and S. Kandeepan, “Cooperative Fusion Based Passive Multistatic Radar Detection,” *Sensors*, vol. 21, no. 9, Art. no. 3209, 2021 https://doi.org/10.3390/s21093209

[4] R. Plšek, V. Stejskal, M. Pelant and M. Vojáček, "Passive Coherent Location and Passive ESM tracker systems synergy," *2013 14th International Radar Symposium (IRS)*, Dresden, Germany, 2013, pp. 149-154

[5] Y. Hu, J. Yi, X. Wan and F. Cheng, "Target Localization and Measurement Association in PCL-PET Hybrid Heterogeneous Network," in *IEEE Transactions on Aerospace and Electronic Systems*, vol. 61, no. 2, pp. 3261-3272, April 2025 https://doi.org/10.1109/taes.2024.3486263

[6] M. Malanowski, J. Kochański and R. Owczarek, "Passive Location System as a combination of PCL and PET technologies," *2022 IEEE Radar Conference (RadarConf22)*, New York City, NY, USA, 2022, pp. 1-6

[7] T. Brenner, P. Kasprzak and L. Lamentowski, "Position estimation in the multiband PCL-PET fusion system," *2014 15th International Radar Symposium (IRS)*, Gdansk, Poland, 2014, pp. 1-4, https://doi.org/10.1109/IRS.2014.6869282

[8] M. Konopko, L. Lamentowski, W. Dyszynski and T. Brenner, "Analysis of Measurement Association Methods in PCL-PET Passive Location System", *2018 19th International Radar Symposium (IRS)*, Bonn, Germany, 2018, pp. 1-8, https://doi.org/10.23919/IRS.2018.8448243

[9] L. Lamentowski, T. Brenner and M. Nieszporski, "De-ghosting and target extraction algorithm analysis for the PCL-PET fusion system," *2015 16th International Radar Symposium (IRS)*, Dresden, Germany, 2015, pp. 48-53, https://doi.org/10.1109/IRS.2015.7226361

[10] T. Brenner, W. Dyszynski and L. Lamentowski, "Cluster analysis for multistatic passive combined PCL and PET fusion system," *2018 22nd International Microwave and Radar Conference (MIKON)*, Poznan, Poland, 2018, pp. 595-596, https://doi.org/10.23919/MIKON.2018.8405296

[11] G. Krawczyk, "Strategies for target localization in passive bistatic radar," *2016 17th International Radar Symposium (IRS)*, Krakow, Poland, 2016, pp. 1-6, https://doi.org/10.1109/IRS.2016.7497382

[12] N. Misaghi, M. Parker and B. Ng, "Target Localisation in Real Time for Non-Coherent Multistatic Passive Radar," *2024 International Radar Conference (RADAR)*, Rennes, France, 2024, pp. 1-6, https://doi.org/10.1109/RADAR58436.2024.10993622

[13] L. Lamentowski, R. Mularzuk, T. Brenner and M. Nieszporski, "Tracking algorithm analysis for the PCL-PET fusion system," *2015 Signal Processing Symposium (SPSympo)*, Debe, Poland, 2015, pp. 1-6, https://doi.org/10.1109/SPS.2015.7168274

[14] T. Brenner, P. Kasprzak and L. Lamentowski, "Tracking algorithm in the multiband PCL-PET fusion system," *2014 15th International Radar Symposium (IRS)*, Gdansk, Poland, 2014, pp. 1-5, https://doi.org/10.1109/IRS.2014.6869283

[15] M. Malanowski, K. Kulpa and R. Suchozebrski, "Two-stage tracking algorithm for passive radar," *2009 12th International Conference on Information Fusion*, Seattle, WA, USA, 2009, pp. 1800-1806

[16] M. Malanowski "Signal Processing for Passive Bistatic Radar", Artech House, pp. 10

[17] Chalise, R., S. K. Sharma, and R. J. Marks II, "Target localisation in a multi-static passive radar system," *Signal Processing*, vol. 104, pp. 168–179, 2014, https://doi.org/10.1016/j.sigpro.2014.02.023

[18] N. H. Nguyen, K. Doğançay "Signal Processing for Multistatic Radar Systems", Academic Press, pp. 143-148.

[19] P. Szelągowski, "Numerical Method of Position Estimation for Multistatic Passive Radar," *2024 International Radar Symposium (IRS)*, Wroclaw, Poland, 2024, pp. 325-329.

[20] P. Szelągowski, M. Dróżka, "Grid-Based Spatial Localization Concept for Multistatic Passive Radar System," *2025 Signal Processing Symposium (SPSympo)*, Warsaw, Poland, 2025, pp. 159-164, https://doi.org/10.23919/SPSympo63739.2025.11123978

[21] W. H. Foy "Position-Location Solutions by Taylor-Series Estimation" IEEE Transactions on aerospace and electronic systems, 1976.

[22] N.H. Bingham, J.M. Fry, "Regression: Linear Models in Statistics", Springer Undergraduate Mathematics Series, 2010, pp. 73. https://doi.org/10.1007/978-1-84882-969-5

[23] K. Levenberg, "A method for the solution of certain non-linear problems in least squares," Quarterly of Applied Mathematics, vol. 2, no. 2, pp. 164–168.

[24] D. P. Bertsekas, "Nonlinear Programming", 3rd ed., Belmont, MA, USA: Athena Scientific, 2016, pp. 19–35

[25] D. W. Marquardt, "An algorithm for least-squares estimation of nonlinear parameters," SIAM Journal of Applied Mathematics, vol. 11, no. 2, pp. 431–441, https://doi.org/10.1137/0111030

[26] P. Misra, P. Enge, "Global Positioning System: Signals, Measurements, and Performance", 2nd ed., Lincoln, MA, USA: Ganga-Jamuna Press, 2006, pp. 208

[27] M. Malanowski, M. Żywek and Ł. Maślikowski, "Investigation of Altitude Estimation Accuracy in Passive Radar," *2025 IEEE International Radar Conference (RADAR)*, Atlanta, GA, USA, 2025, pp. 1-6, https://doi.org/10.1109/RADAR52380.2025.110